

# JGR Space Physics



## RESEARCH ARTICLE

10.1029/2023JA031810

### Key Points:

- Studying Flux Transfer Events (FTEs) can give information about the properties of magnetic reconnection on Mercury's dayside magnetopause
- Most reconnection sites of modeled FTEs are found to pass through points of high-magnetic shear on the magnetopause
- Find evidence of low-shear reconnection at shear angles  $<70^\circ$ , suggesting reconnection may not be confined to points of maximal shear

### Supporting Information:

Supporting Information may be found in the online version of this article.

### Correspondence to:

S. Zomerdijk-Russell,  
[sophia.zomerdijk-russell16@imperial.ac.uk](mailto:sophia.zomerdijk-russell16@imperial.ac.uk)

### Citation:

Zomerdijk-Russell, S., Masters, A., Sun, W. J., Fear, R. C., & Slavin, J. A. (2023). Does reconnection only occur at points of maximum shear on Mercury's dayside magnetopause? *Journal of Geophysical Research: Space Physics*, 128, e2023JA031810. <https://doi.org/10.1029/2023JA031810>






Received 26 JUN 2023

Accepted 7 OCT 2023

©2023. The Authors.

This is an open access article under the terms of the [Creative Commons Attribution License](https://creativecommons.org/licenses/by/4.0/), which permits use, distribution and reproduction in any medium, provided the original work is properly cited.

## Does Reconnection Only Occur at Points of Maximum Shear on Mercury's Dayside Magnetopause?

S. Zomerdijk-Russell<sup>1</sup> , A. Masters<sup>1</sup> , W. J. Sun<sup>2,3</sup> , R. C. Fear<sup>4</sup> , and J. A. Slavin<sup>2</sup> 

<sup>1</sup>The Blackett Laboratory, Imperial College London, London, UK, <sup>2</sup>Department of Climate and Space Sciences and Engineering, University of Michigan, Ann Arbor, MI, USA, <sup>3</sup>Space Sciences Laboratory, University of California, Berkeley, Berkeley, CA, USA, <sup>4</sup>School of Physics and Astronomy, University of Southampton, Southampton, UK

**Abstract** MESSENGER observations of large numbers of flux transfer events (FTEs) during dayside crossings of Mercury's magnetopause have shown that the highly dynamic Hermean magnetosphere is strongly driven by frequent and intense magnetic reconnection. Since FTEs are products of reconnection, study of them can reveal information about whether reconnection sites favor points of maximum shear on the magnetopause. Here, we analyze 201 FTEs formed under relatively stable upstream solar wind conditions as observed by MESSENGER during inbound magnetopause crossings. By modeling paths of these FTEs along the magnetopause, we determine the conditions and locations of the reconnection sites at which these FTEs were likely formed. The majority of these FTE formation paths were found to intersect with high-magnetic shear regions, defined as shear angles above  $135^\circ$ . Seven FTEs were found where the maximum shear angle possible between the reconnecting magnetic field lines was less than  $80^\circ$  and three of these had shear angles less than  $70^\circ$ , supporting the idea that very low-shear reconnection could be occurring on Mercury's dayside magnetopause under this global-scale picture of magnetic reconnection. Additionally, for the FTEs formed under these low-shear reconnection conditions, tracing a dominant X-line connecting points of maximum shear along the magnetopause that passes through a region of very low-shear may be difficult to justify, implying reconnection could be occurring anywhere along Mercury's magnetopause and may not be confined to points of maximum shear.

**Plain Language Summary** Like at Earth, a magnetic field is generated in Mercury's iron core and this field forms a structure, known as a magnetosphere, around the planet that protects it from the stream of charged particles ejected from the Sun. Mercury's magnetosphere is driven by magnetic reconnection processes, where magnetic field lines from the Sun and Mercury's own field “break” and reconfigure. During this reconnection process, helical magnetic field structures termed magnetic flux ropes (FRs) can form. At Mercury, these FRs are of particular interest as they occur in large numbers suggesting reconnection occurs more frequently in the Mercury system than at Earth. We here analyze and model 201 of these FRs, using data from the MESSENGER mission, to investigate under what conditions the reconnection that formed these FRs occurred. We find for the majority of the FRs the maximum magnetic shear angle between the reconnecting field lines is larger than  $135^\circ$ , suggesting most form under higher shear conditions, as expected. However, we find a small number of cases where the shear angles between the reconnecting field lines is much lower than expected, supporting the idea that magnetic reconnection processes occur much more easily at Mercury.

## 1. Introduction

The global intrinsic magnetic field of Mercury was first discovered when the Mariner 10 spacecraft made 3 flybys of the planet in the 1970s (Ness et al., 1974, 1975). Subsequently, on 18 March 2011, the MErcury Surface, Space ENvironment, GEOchemistry, and Ranging (MESSENGER) probe became the first spacecraft to be inserted into orbit around Mercury and spent four Earth years observing the planet's electromagnetic environment (Johnson et al., 2012; Solomon et al., 2007). Observations made by MESSENGER determined Mercury's intrinsic magnetic field is highly dipolar, with a dipole magnetic moment of  $190 \pm 10$  nT  $R_M^3$  (where  $R_M = 2439.7$  km is Mercury's radius) that is offset northward by  $0.196 R_M$  (Anderson et al., 2008, 2012; Johnson et al., 2012). Due to Mercury's proximity to the Sun, this weak intrinsic field of the terrestrial planet is exposed to a strong interplanetary magnetic field (IMF) embedded in a dense and hot solar wind. As such, Mercury supports a small but highly dynamic magnetosphere that is strongly driven by the solar wind (e.g., Dibaccio et al., 2013; Imber et al., 2014; Slavin et al., 2021; Zhong et al., 2015; Zomerdijk-Russell, Masters, Korth, & Heyner, 2023).

Magnetic reconnection plays an essential factor in interactions between the solar wind and a planetary magnetosphere. Reconnection between the intrinsic planetary field lines and the IMF draped over the magnetopause has been shown to erode Mercury's dayside magnetopause (Heyner et al., 2016; Slavin, Anderson, et al., 2010) and drive magnetic flux circulation in the Dungey cycle (Dungey, 1961). At Earth's dayside magnetopause, pressure equilibrium of the total pressure internal and external to the magnetosphere controls the magnetopause location. However, "asymmetric" reconnection is often dominant, where the magnetospheric field strength is much larger than the magnetosheath field strength leading to a large difference in the magnetic pressure across the magnetopause boundary and, hence, a larger plasma  $\beta$  difference. This results in diamagnetic drift suppression of component reconnection and antiparallel configurations of the reconnecting magnetic fields are favored (i.e., the magnetic shear angle between the magnetosheath and magnetospheric fields approaches  $180^\circ$ ). Therefore, at Earth, reconnection on the dayside magnetopause usually occurs at low-latitudes where the shear angle between the reconnecting field lines is maximized along a region referred to as the dominant X-line and rates of reconnection are typically slower (Dungey, 1961; Fuselier et al., 2021; Sonnerup, 1974; Sonnerup et al., 1981; Swisdak & Drake, 2007; Trattner et al., 2007).

At Mercury, however, the magnetosheath and magnetospheric fields are comparable, therefore, it is expected that "symmetric" reconnection will be dominant and there will be less severe diamagnetic drift suppression. As a result, magnetic reconnection on Mercury's dayside magnetopause is predicted to occur at faster rates and over a wider range of magnetic shear angles and locations on the magnetopause than that at Earth. This expectation of faster reconnection rates is confirmed by observations of reconnection at Mercury, discussed further below (e.g., Dibraccio et al., 2013; Slavin et al., 2014).

During magnetic reconnection, open field lines are convected away from the reconnection site due to magnetosheath flow and magnetic forces of the field lines and, additionally, can form into helical bundles of flux. These structures are called magnetic flux ropes (FRs) and it is thought they are formed between multiple neighboring reconnecting X-lines (Lee & Fu, 1985) or by sequential X-line reconnections (Raeder, 2006), and were first observed at Earth's magnetopause by Haerendel et al. (1978) and Russell and Elphic (1978). At the dayside magnetopause, these FRs are referred to as flux transfer events (FTEs) and have since been observed in the magnetospheres of Jupiter (Walker & Russell, 1985), Saturn (Jasinski et al., 2016) and Mercury (Russell & Walker, 1985). As FTEs are generated by magnetic reconnection between the IMF and magnetospheric field lines, in the core of an FTE one end of the FR's magnetic field lines will be connected to the solar wind while the other is connected to the magnetosphere. In spacecraft observations, these FTE-type FRs are seen as a bipolar signature in the field component normal to the magnetopause boundary that is coupled with an enhancement in the magnetic field strength (Lee & Fu, 1985), and have been found to be on the order of 1 min in length and separated by 10's of minutes in the magnetospheres of Earth (Lockwood et al., 1995), Jupiter (Walker & Russell, 1985) and Saturn (Jasinski et al., 2021).

Observations of FTEs at Mercury, have, however, shown that FTE-type FRs will last only on the order of 1 s, occur extremely frequently, with spacings of  $\sim 10$  s in spacecraft observations, and often appear in numbers of 10 or more within a few minutes, in events referred to as FTE showers (Slavin et al., 2009, 2010a, 2010b, 2012, 2014; Imber et al., 2014; Sun et al., 2020). Since FTEs are known to be reconnection-related phenomenon the study of them has shown that Mercury's magnetosphere is a strongly reconnection-driven system, as expected (Slavin et al., 2021; Sun et al., 2022; and references therein). This enhanced reconnection-driven formation of FTEs observed is likely due to the low solar wind Alfvénic Mach number environment at Mercury's orbit (Slavin & Holzer, 1979) and comparable intensities between the IMF and Mercury's intrinsic planetary field leading to "symmetric" reconnection being the dominant process (Dibraccio et al., 2013; Slavin et al., 2014). These strong interactions can lead to a low plasma  $\beta$  magnetosheath and magnetic flux piling up sunward of the magnetopause, forming a thick plasma depletion layer favorable for high reconnection rates (Dibraccio et al., 2013; Gershman et al., 2013; Swisdak et al., 2003). FTEs can be used to reveal more information about the occurrence and properties of magnetic reconnection in the Hermean magnetospheric system and could allow testing of the hypothesis that, since diamagnetic drift suppression is less severe in the Mercury system, reconnection can occur over a wider range of magnetic shear angles and may not be confined to points of maximal shear on Mercury's magnetopause.

A large statistical survey by Leyser et al. (2017) showed FTE formation at Mercury exhibits a strong dependence on the IMF's orientation. Reconnection rates were found to be enhanced for MESSENGER magnetopause

crossings during southward oriented IMF, for which the magnetic shear angle across the dayside magnetopause is larger, reflecting what has been observed at Earth (e.g., Paschmann et al., 1986; Phan et al., 2013). Simulations of FTEs at Mercury using Hall magnetohydrodynamic, embedded particle in cell and global hybrid models have also shown that the rate of FTE production shows a strong dependence on Alfvénic Mach number and IMF orientation in good agreement with MESSENGER results (Guo et al., 2021; Li et al., 2023; Lu et al., 2022). These results have shown FTE occurrence is higher under southward IMF conditions, however, FTE showers have also been observed under northward IMF on Mercury's dayside magnetopause (Leyser et al., 2017; Slavin et al., 2014; Sun et al., 2020), suggesting reconnection-driven formation of FTEs on the dayside magnetopause could be occurring over a wider range of magnetic shear angles than those typically observed at Earth (e.g., Phan et al., 2013).

By modeling FTE-type FRs observed by the MESSENGER spacecraft during steady inbound magnetopause crossings, we here determine where FTEs can be generated on Mercury's dayside magnetopause and under what magnetic shear angle conditions their reconnection-driven formation could have occurred. We assess if the reconnection sites are in regions of maximum shear like those expected at Earth, or whether, due to enhanced reconnection rates at Mercury, FTEs can be formed under lower shear conditions at points across the dayside magnetopause that are not confined to maximal shear regions.

## 2. Identification of FTEs in MESSENGER Data Suitable for Modeling

In this study, we utilized the Sun et al. (2020) list of 1,953 MESSENGER magnetopause crossings associated with observations of FTE showers. Sun et al. (2020) used an established technique for automatic detection of FRs (Smith, Slavin, Jackman, Fear, et al., 2017) to identify FTE-type FRs within a few minutes either side of a MESSENGER magnetopause crossing. The automatic FR detection technique applies a continuous wavelet transform to locate significant, considered to be greater than one standard deviation, bipolar deflections in the magnetic field component normal to the magnetopause boundary coincident with enhancements in the total field strength and other magnetic field components. Magnetic field measurements around the deflections were fitted to a cylindrical force-free flux rope model. Further applications and details of this technique can be found in Smith, Jackman, Frohmaier, Coxon, et al. (2018), Smith, Jackman, Frohmaier, Fear, et al. (2018), Smith, Slavin, Jackman, Fear, et al. (2017), and Smith, Slavin, Jackman, Poh, et al. (2017). The initial aim of this study was to use these MESSENGER observations of FTE-type FRs and the associated upstream solar wind conditions to determine the locations at which reconnection could be occurring on Mercury's magnetopause. To ensure the solar wind conditions measured by MESSENGER during a magnetopause crossing reflected the conditions under which the FTE-type could have been formed, we required inbound passes of the magnetosphere that were associated with relatively steady upstream conditions. Under these more stable conditions, and due to the high velocities of FTE-type FRs at Earth, that are expected to be even higher at Mercury, and the small spatial scale of Mercury's magnetosphere, it could reasonably be assumed the upstream solar wind conditions had not significantly changed from the time of the FTE-type FRs formation to its observation.

From the Sun et al. (2020) list of MESSENGER magnetopause crossings associated with FTEs, a subset of inbound crossings where the magnetic field conditions upstream of the magnetopause were considered to be "steady" were identified. For each inbound pass, an interval of a few minutes upstream of the magnetopause was determined. The length of this interval was calculated using the time the solar wind took to propagate through the length of the magnetopause's standoff distance multiplied by a large, arbitrary confidence factor of 30. The confidence factor was chosen to ensure the length of this time interval was on the order of the typical time taken for Mercury's magnetosphere to reconfigure, that is, the Dungey cycle timescale (Slavin et al., 2009), and our results were found to be insensitive to this choice, with the length of the intervals upstream varying little between events. Figure 1a shows components of magnetic field measurements made by MESSENGER during an inbound pass on 15 December 2013, where a clear rotation in the magnetic field indicates the magnetopause crossing, marked by the vertical dashed red line. These magnetic field components are in the Cartesian Mercury Solar Magnetospheric (MSM) coordinate system, where positive  $x_{\text{MSM}}$  points toward the Sun from the center of Mercury's magnetic dipole, positive  $z_{\text{MSM}}$  is aligned with magnetic north and normal to the orbital plane of Mercury, and positive  $y_{\text{MSM}}$  completes the right-handed system. The determined interval upstream of the magnetopause, in the magnetosheath region, is shown by the darker gray shaded area in Figure 1a and an interval of the same length downstream of the magnetopause, in the magnetosphere, is highlighted in light gray. The clock angle between the  $B_y$  and  $B_z$  magnetic

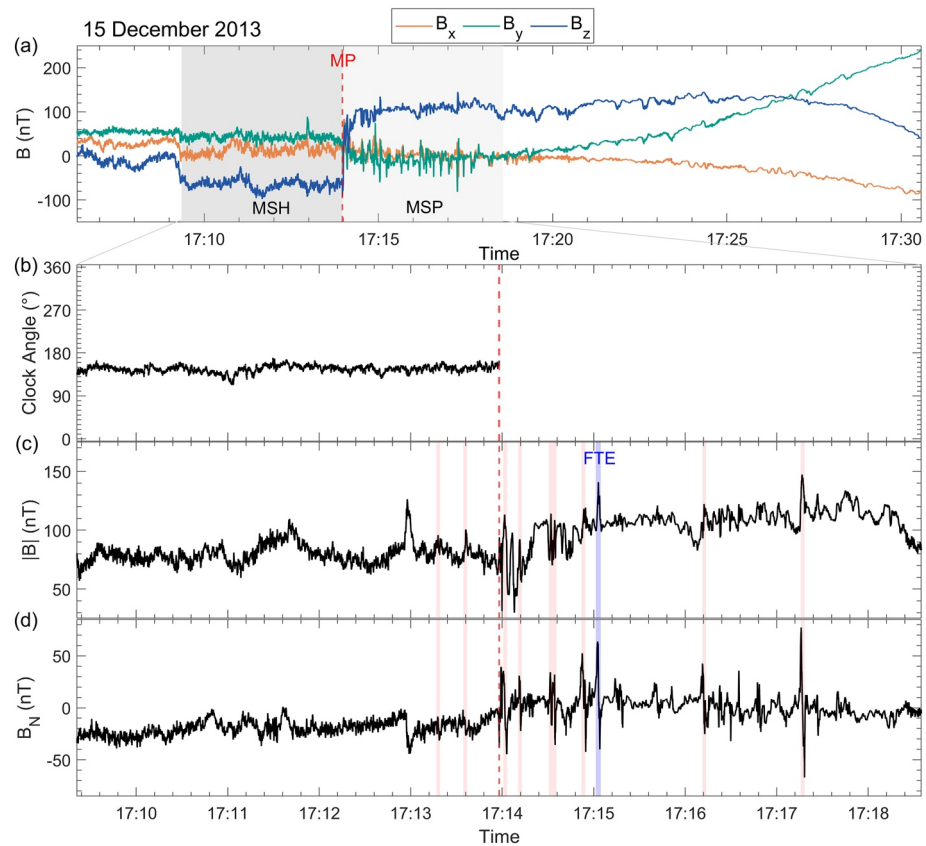


**Figure 1.** An example of a dayside inbound pass made by MESSENGER on 15 December 2013. (a) Time series of the magnetic field components measured by the spacecraft's magnetometer in MSM coordinates are shown in orange ( $B_x$ ), green ( $B_y$ ) and blue ( $B_z$ ). The vertical dashed red lines indicate the magnetopause location. The gray shaded areas indicate regions of interest zoomed in on in panels (b)–(d). (b) Time series of the magnetic field's clock angle in the region upstream of the magnetopause calculated using the  $B_y$  and  $B_z$  components. Time series of (c) the magnetic field magnitude and (d) the magnetic field component normal to the magnetopause surface ( $B_N$ ). The vertical blue line marks an FTE-type flux rope selected to be modeled and the vertical red lines indicate additional FTE-type flux ropes.

field components was then calculated in the region upstream of the magnetopause, shown in Figure 1b and the standard deviation ( $\sigma$ ) in this clock angle was determined.

Magnetopause crossings where  $\sigma < 12^\circ$  were categorized as “steady” and 201 of these steady, inbound magnetopause crossings were found. This standard deviation threshold was chosen to allow upstream solar wind conditions to be as well constrained as possible with the limitations on information about the simultaneous upstream conditions during MESSENGER observations of the FTEs. Whilst this choice of standard deviation threshold possibly omitted magnetopause crossing events with particularly strong FTEs, the number of FTEs per magnetopause crossing and magnetosheath plasma  $\beta$  values were found to reflect the trends seen in the Sun et al. (2020) full data set. Additionally, the key results presented in this paper were found to be insensitive to the choice of standard deviation threshold.

The 201 MESSENGER steady, inbound magnetopause crossings identified were crossings that had been categorized by Sun et al. (2020) as those containing signatures of FTE-type FRs. Figures 1c and 1d show the magnetic field magnitude ( $|B|$ ) as measured by MESSENGER and the magnetic field component projected in the direction normal to the magnetopause surface ( $B_N$ ), resolved from a parabolic magnetopause model (Alexeev et al., 2008) and standoff distance from the MESSENGER observation of the magnetopause crossing (Winslow et al., 2013), see Section 3.1. In Figure 1c it can be seen that the ratio of the upstream magnetosheath field magnitude to the downstream magnetospheric field magnitude is approximately 1. The average ratio between the upstream and downstream fields for all 201 crossings was found to be  $\sim 0.78$ , implying highly “symmetric” reconnection is occurring at Mercury's magnetopause, which is predicted to lead to high rates of reconnection (e.g., Gershman et al., 2013; Slavin & Holzer, 1979).

FTE-type FRs, identified by a bipolar signature in  $B_N$  and an enhancement in  $|B|$ , are highlighted in Figures 1c and 1d by the vertical red and blue lines. On average,  $\sim 25$  FTEs were observed in the selected intervals upstream and downstream of the magnetopause for the 201 magnetopause crossing events. These observations of high rates of reconnection are consistent with those expected from the observed symmetric reconnection conditions. For every magnetopause crossing event, we then selected one unambiguous FTE-type FR from within the chosen intervals upstream and downstream of the magnetopause to be modeled, the blue vertical line in Figures 1c and 1d, and also noted the polarity of its bipolar signature in the  $B_N$  component. It was found that all FTEs in the intervals produced very similar results when modeled, therefore, the choice of an unambiguous FTE to be modeled was arbitrary. This resulted in a list of 201 FTE-type FR signatures associated with steady, inbound passes of Mercury's magnetosphere that could then be modeled and further investigated.

### 3. Modeling Locations of Possible FTE Formation Reconnection Sites: 15 December 2013 FTE Case Study

The next aim of this study was to model where FTE-type FRs were most likely to have formed on Mercury's magnetopause and understand under what conditions this reconnection-driven formation occurred. The FTE observed on 15 December 2013 was selected as a case study to model first, as it was formed under a near southward IMF orientation that at Mercury can typically result in reconnection processes on the dayside magnetopause. To model the FTE observed on 15 December 2013, we determined how the FTE-type FR had moved along the magnetopause from the point of formation at a reconnection site to the point of observation by MESSENGER (blue vertical line in Figures 1c and 1d). We used a combination of different analytical descriptions of both external magnetosheath and internal magnetospheric parameters adjacent to Mercury's magnetopause to build our model and similar methods have been used by Fear et al. (2007), for example, in Earth's magnetosphere.

To model FR motion over a magnetopause surface in response to solar wind flow and magnetic forces resulting from magnetic reconnection, the approach of Cooling et al. (2001) can be used. The Cooling modeling approach allows the instantaneous velocity of an FTE-type FR to be calculated based on input solar wind and magnetosheath conditions. Following reconnection, two, separate open FRs are formed and their instantaneous velocities are in the de Hoffman-Teller frame (de Hoffmann & Teller, 1950). The de Hoffman-Teller velocities were derived by Cowley and Owen (1989) to be:

$$\underline{v}_{HTN} = \underline{v}_{MSH} - v_A \underline{B}_{MSH} \quad (1)$$

$$\underline{v}_{HTS} = \underline{v}_{MSH} + v_A \underline{B}_{MSH} \quad (2)$$

where  $\underline{v}_{HTN}$  and  $\underline{v}_{HTS}$  are good approximations of the velocities of the FRs connected to the northern and southern cusps respectively (Fear et al., 2007, 2009). In our model, as we must start at the location of observation of the FTE by MESSENGER, we instead used the de Hoffman-Teller speeds to step backwards in time along the magnetopause to find where along the surface the reconnection site that formed the FTE could be located. We first consider two paths along the magnetopause that the FTE-type FR could have formed anywhere along and then followed to the point of observation, hereafter referred to as "FTE formation paths." Two paths are considered initially since a pair of flux tubes is opened during reconnection and the flux tube associated with the observed FTE could be either of the pair and connected to the northern or southern cusp with an instantaneous velocity of  $\underline{v}_{HTN}$  or  $\underline{v}_{HTS}$ . Figure 2 shows a schematic representation of the de Hoffman-Teller velocities used to step backwards in time that is, with a negative velocity, from the FTE observation point to determine the initial two possible FTE formation paths on the magnetopause (cyan lines). The de Hoffman-Teller velocities are dependent on external magnetosheath parameters, the magnetosheath flow velocity, magnetic field and Alfvén speed. Therefore, we used the following analytical approaches to estimate these parameters.

#### 3.1. Global Shape of Magnetopause Boundary and Mercury's Magnetospheric Field

First, a parabolic surface was used to describe the global shape of the magnetopause boundary (Alexeev et al., 2008; Cooling et al., 2001; Kobel & Flückiger, 1994; Winslow et al., 2013). The paraboloid, with revolution about the  $x_{MSM}$ -axis, is given by



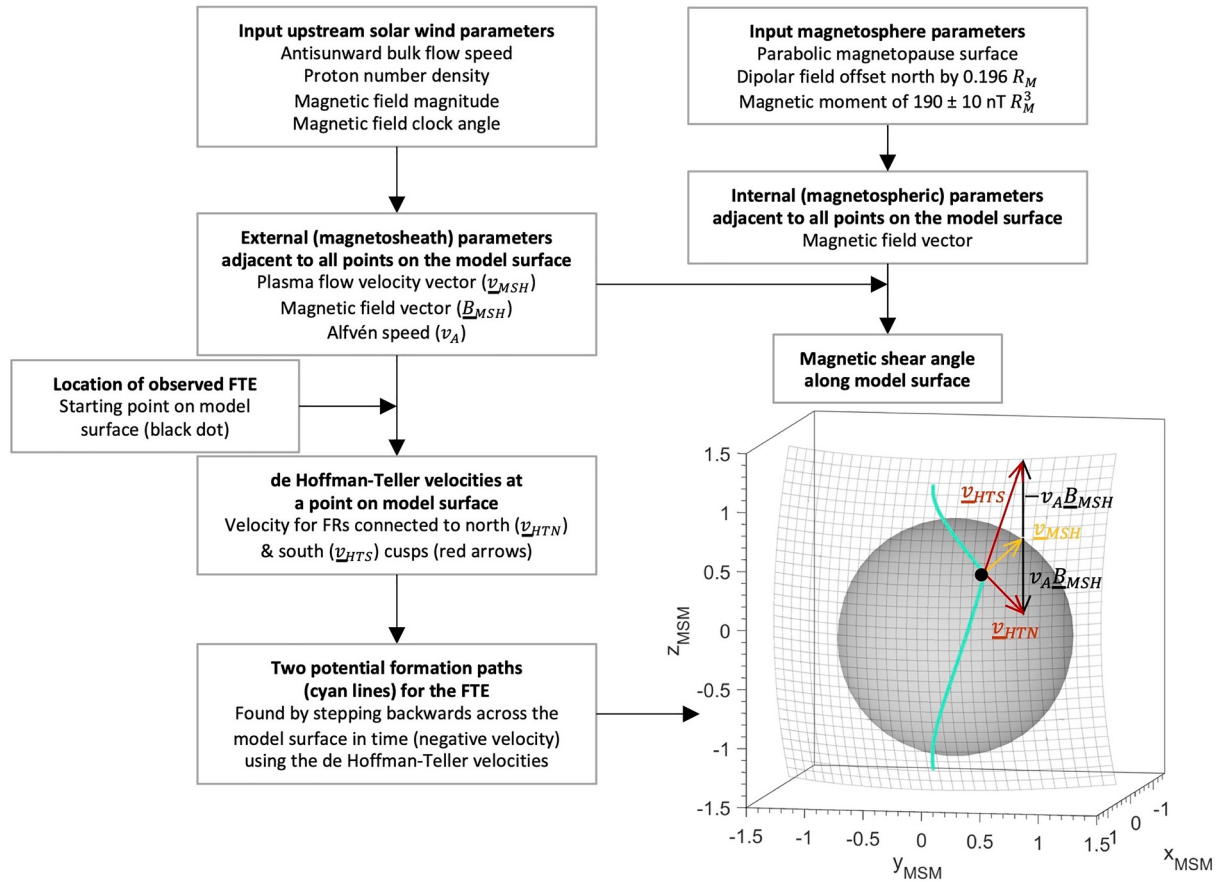


**Figure 2.** A schematic illustration of the model used to determine possible FTE formation reconnection sites.

$$y_{\text{MSM}}^2 + z_{\text{MSM}}^2 = 2R_{\text{MP}}(R_{\text{MP}} - x_{\text{MSM}}), \quad (3)$$

where  $R_{\text{MP}}$  is the magnetopause standoff distance, determined from the location at which MESSENGER crossed the magnetopause boundary during its inbound pass. Additionally, throughout our modeling approach aberration effects are accounted for at Mercury by determining the aberration angle at the time of MESSENGER's observation of the FTE, using Kepler's Laws of planetary motion, and transforming the observation locations into an aberrated frame.

In this work, the intrinsic magnetic field of Mercury is modeled as a dipole with a magnetic moment of  $190 \pm 10 \text{ nT } R_M^3$  offset north of the equatorial plane by  $0.196 R_M$ . The magnetic field's direction just inside of the magnetopause is computed by setting the component in the direction that is locally normal to the parabolic magnetopause boundary to zero (Masters, 2014).

### 3.2. Magnetosheath Flow Velocity

For the magnetosheath flow velocity parameter required in Equations 1 and 2, we used expressions derived by Petrinec and Russell (1997) for the hydrodynamic case. The following equation allowed the initial magnetosheath flow velocity speed ( $v_{\text{MSH}}$ ) to be determined at any point on the magnetopause surface,

$$v_{\text{MSH}} = v_u \sqrt{\frac{(M_S^2 + 3)}{M_S^2} \left( 1 - \left( \cos^2 \psi + \frac{3}{4} \frac{(5M_S^2 - 1)^{3/2}}{M_S^5} \sin^2 \psi \right)^{2/5} \right)}, \quad (4)$$

where  $v_u$  is the solar wind flow speed upstream of the bow shock,  $M_s$  is the upstream solar wind sonic Mach number and  $\psi$  is the angle between the local normal to the magnetopause surface and the  $x$ -axis (the flaring angle). The solar wind flow speed and sonic Mach number were determined using averages of the solar wind plasma conditions (Diego et al., 2020), upstream of the magnetopause, due to limitations on information about ambient plasma from MESSENGER measurements. Uncertainties were tied into these upstream plasma condition estimates as discussed in Section 3.5. Additionally, Equation 4 assumes that magnetic forces are negligible, which is a good approximation when the magnetosheath magnetic field is weak. At Mercury, however, the magnetosheath field is larger and more comparable to the magnetospheric field, therefore, it is expected that magnetic tension forces will act to accelerate the magnetosheath flow around the obstacle of the magnetopause boundary (Petrinec & Russell, 1997). Nevertheless, this effect is anticipated to be small and, since, the upstream conditions are poorly constrained, any increase to the flow speed is likely consumed by the large uncertainties in the upstream solar wind conditions and hence, the magnetosheath flow speed already treated and discussed in Section 3.5. To determine the velocity of the magnetosheath flow at any point on the magnetopause, we assumed the initial magnetosheath flow velocity field points radially away from the subsolar point and is parallel to the magnetopause surface at all points across the boundary.

### 3.3. Magnetosheath Magnetic Field

The magnetosheath magnetic field ( $B_{X_{MSH}}, B_{Y_{MSH}}, B_{Z_{MSH}}$ ) at any point just outside of the magnetopause boundary ( $X, Y, Z$ ) was also required for the de Hoffman-Teller velocities (Equations 1 and 2). By draping an IMF ( $B_{X_{IMF}}, B_{Y_{IMF}}, B_{Z_{IMF}}$ ) with given clock angle orientation over a parabolic magnetopause, the magnetosheath field direction was determined using the analytical equations of Kobel and Flückiger (1994),

$$B_{X_{MSH}} = -A \left[ -B_{X_{IMF}} \left( 1 - \frac{R_{MP}}{2l} \right) + B_{Y_{IMF}} \left( \frac{Y}{l} \right) + B_{Z_{IMF}} \left( \frac{Z}{l} \right) \right], \quad (5)$$

$$B_{Y_{MSH}} = A \left[ -B_{X_{IMF}} \left( \frac{Y}{2l} \right) + B_{Y_{IMF}} \left( 2 - \frac{Y^2}{l R_{MP}} \right) - B_{Z_{IMF}} \left( \frac{YZ}{l R_{MP}} \right) \right], \quad (6)$$

$$B_{Z_{MSH}} = A \left[ -B_{X_{IMF}} \left( \frac{Z}{2l} \right) - B_{Y_{IMF}} \left( \frac{YZ}{l R_{MP}} \right) + B_{Z_{IMF}} \left( 2 - \frac{Z^2}{l R_{MP}} \right) \right], \quad (7)$$

where

$$A = \frac{2R_{BS} - R_{MP}}{2(R_{BS} - R_{MP})}, \quad (8)$$

$l$  is the distance from the focus to the magnetopause surface,

$$l = \frac{3R_{MP}}{2} - X, \quad (9)$$

and  $R_{MP}$  and  $R_{BS}$  are the magnetopause and bow shock standoff distances, respectively. The IMF clock angle orientation was determined from the MESSENGER measurements of the magnetosheath field in the interval just upstream of the magnetopause, that is, the dark gray shaded region in Figure 1a. Using the location at which MESSENGER crossed Mercury's magnetopause (red vertical dashed line in Figure 1) and measurements of the magnetosheath magnetic field in the clock angle direction ( $B_y$  and  $B_z$  components only with  $B_x$  set to be zero), we rearranged Equations 5–7, to find the orientation of the IMF for each field measurement in the interval upstream of the magnetopause. Whilst the  $B_x$  component of the IMF magnetic field vector can be significant at the Earth and Mercury, this component is generally ignored to allow the simple but adequate model of Kobel and Flückiger (1994) to be used to determine the IMF's draping pattern over the magnetopause (e.g., Cooling et al., 2001; Vandas et al., 2020; Zomerdijk-Russell et al., 2021). The IMF orientations from the interval upstream of the magnetopause were then used as inputs to the Kobel and Flückiger (1994) magnetosheath field model to find the direction of the draped magnetosheath field at any point just outside of the magnetopause surface for each measurement in the upstream interval.

### 3.4. Alfvén Speed

The final parameter that the de Hoffman-Teller velocities (Equations 1 and 2) depend on is the Alfvén speed of the system given by,

$$v_A^2 = \frac{B_{\text{MSH}}^2}{\mu_0 \rho_{\text{MSH}}}, \quad (10)$$

where  $\mu_0$  is the permeability of free space,  $\rho_{\text{MSH}}$  is the mass density of the magnetosheath and  $B_{\text{MSH}}$  is the magnetosheath field magnitude. The magnetosheath mass density was calculated using

$$\rho_{\text{MSH}} = \rho_u \frac{4^{\frac{8}{5}} M_S^2}{(M_S^2 + 3)(5M_S^2 - 1)^{\frac{3}{2}}} \left[ \frac{4^{\frac{4}{5}} M_S^5 \cos^2 \psi + (5M_S^2 - 1)^{\frac{3}{2}} \sin^2 \psi}{3^{\frac{5}{2}}} \right]^{\frac{3}{5}}, \quad (11)$$

where  $\rho_u$  is the solar wind mass density upstream of the bow shock (Petrinec & Russell, 1997). To find the magnitude of the magnetosheath magnetic field, MESSENGER measurements of the magnetic field magnitude in the interval upstream were used (Figure 1c).

### 3.5. Accounting for Uncertainties in the Upstream Solar Wind Conditions

A simultaneous measurement of the upstream solar wind conditions during MESSENGER's observation of the FTE-type FR on 15 December 2013 was not possible, therefore, uncertainties needed to be tied into our modeled FR trajectories along the magnetopause. The locations of the FRs' paths on the magnetopause surface depend on four upstream parameters that cannot be measured at the same time the observation was made, the orientation (reliant on the IMF orientation, see Equations 5–7) and magnitude of the magnetosheath field (Equation 10), and the solar wind speed (Equation 4) and mass density (Equation 11).

To find formation paths for the FTE-type FR observed by MESSENGER on 15 December 2013, we used orientations of the IMF from the MESSENGER magnetosheath measurements made in the interval upstream of the magnetopause as inputs to our model (dark gray shaded region in Figure 1a). It was found that, as expected, the separation of the two de Hoffman-Teller velocity trajectories became larger for a lower solar wind speed and mass density, and a higher magnetosheath field magnitude, whilst the inverse was true for a smaller separation of the paths. To account for uncertainties in these upstream values, we used minimum and maximum estimates to determine two maximally separated FTE formation paths and two minimally separated paths for each IMF orientation (a schematic illustration of this is included in Supporting Information S1). The upstream solar wind values used were taken from averages of unperturbed periods at Mercury's orbit as determined by Diego et al. (2020), due to MESSENGER limitations on information about ambient plasma. The minimum and maximum upstream solar wind speeds ( $\langle v_u \rangle = 384.2 \text{ km s}^{-1}$ ) were 368.8 and 406.2  $\text{km s}^{-1}$ , respectively, and the minimum and maximum solar wind mass densities ( $\langle \rho_u \rangle = 58 \text{ cm}^{-3}$ ) were 44.2 and 69.2  $\text{cm}^{-3}$ , respectively. Values for the maximum and minimum magnetosheath field magnitudes were taken from MESSENGER magnetic field measurements in the interval upstream of the magnetopause (Figure 1c). This resulted in four FTE formation paths on the magnetopause, per IMF orientation, and the reconnection site that generated the FTE-type FR could be located anywhere between the two most extreme paths for each outflow direction.

Values for a magnetosheath plasma  $\beta$  were considered for each of the 201 modeled FTEs. Similar to the Sun et al. (2020) approach to calculate a global plasma  $\beta$ , the magnetosheath thermal pressure was approximated by taking the difference between the magnetosheath and magnetospheric magnetic pressures calculated from the average field strength in the regions upstream and downstream of the magnetopause. The global magnetosheath plasma  $\beta$  values were found to be lower than those typically found at Earth, as shown previously in literature (Sun et al., 2020). However, this approach requires it to be assumed that there is quasi-pressure balance at the magnetopause which can be an over-simplification that does not always hold for certain crossings when the magnetospheric field is larger than the magnetosheath field strength. Additionally, as there are large uncertainties in the upstream magnetosheath field strength at the time of observation of the FTEs, values for the plasma  $\beta$  at local points on the magnetopause surface cannot be well constrained. As such, it is assumed that since estimates of the global magnetosheath plasma  $\beta$  are low, the absolute difference between the magnetosheath and magnetospheric plasma  $\beta$  will be low. Hence, reconnection will likely not be suppressed by the diamagnetic drift condition at any point on Mercury's dayside magnetopause (Phan et al., 2010, 2013; Swisdak et al., 2003, 2010), which matches the high rates of reconnection observed at Mercury (Dibraccio et al., 2013; Imber et al., 2014; Slavin et al., 2009; Slavin, Lepping, et al., 2010).



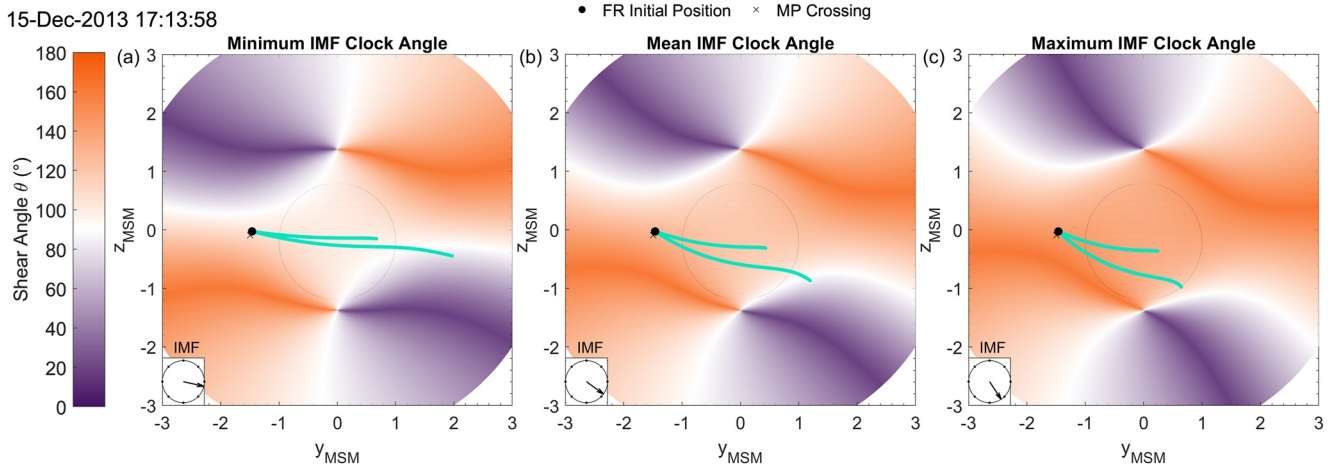


**Figure 3.** FTE-type flux rope formation paths modeled backwards in time on Mercury's magnetopause surface viewed from along the upstream solar wind flow direction using parameters measured by MESSENGER on 15 December 2013. The planet's location is shown by the black circle offset by  $0.2 R_M$  in the negative  $z$  direction, and the parabolic magnetopause surface is set at a standoff distance calculated from the location where MESSENGER crossed the magnetopause (black cross). The location at which MESSENGER observed an FTE-type flux rope is shown by the black dot and the cyan lines denote the modeled FTE formation paths. The (a) minimum, (b) mean and (c) maximum IMF clock angle orientations measured by MESSENGER in the selected region upstream of the magnetopause (Figure 1b) are shown in the inset figures. The color gradient represents the shear angle between the intrinsic magnetic field of Mercury and the magnetosheath magnetic field, found by draping an IMF, with orientation shown in the inset figures, over the magnetopause surface. The reconnection site at which the FTE-type flux rope observed by MESSENGER was formed could be anywhere in the region between the cyan paths.

### 3.6. Using Polarity to Determine the Feasibility of the Modeled Paths

The polarity of the  $B_N$  signature of an FTE-type FR can give information about to which cusp a flux rope is most likely attached, as the polarity is dependent on the motion of the FR relative to the unperturbed magnetic field. For an FTE observed in the magnetosheath, a positive to negative deflection in  $B_N$  (a “standard” (+ to –) polarity) occurs if the FTE's velocity has a component that is antiparallel to the local magnetosheath field, whereas a “reverse” (– to +) polarity will occur if a component of the velocity is parallel to the magnetosheath field (Fear et al., 2007; Rijnbeek et al., 1982). If, however, the FTE is observed inside of the magnetosphere, a standard polarity suggests the FTE's velocity has a component that is parallel to the local intrinsic magnetic field of the planet (Supporting Information S1 includes a schematic illustration of this). For the FTE on 15 December 2013, the FTE-type FR selected to be modeled (vertical blue line in Figures 1c and 1d) was observed in the magnetosphere and had a standard (+ to –) polarity. Therefore, for each IMF orientation, the subsequent two formation paths that had components parallel to the planet's local intrinsic magnetic field were deemed the most feasible.

### 3.7. Modeled Locations of Possible Reconnection Sites on the Magnetopause

Figure 3 shows the modeled locations of the reconnection sites for the FTE observed on 15 December 2013 (Figure 1). Three IMF orientations were selected to be modeled, those associated with the minimum, mean and maximum clock angles in the interval upstream of the magnetopause (Figure 1b). As “steady” inbound crossings had been specifically selected for this study, we could reasonably assume the upstream solar wind conditions had not changed significantly from the time of the FRs formation to its observation. Therefore, by modeling the minimum, mean and maximum cases of the IMF orientation in the upstream interval (shown in the inset figures in Figures 3a–3c, respectively), we encompass the majority of possible IMF orientations that the FTE could have formed under. Hence, for each of the three IMF orientations, we generated two formation paths, incorporating uncertainties in the upstream solar wind values and the FTE's polarity, that the observed FTE could have formed anywhere between.

In Figure 3, the magnetopause is modeled as a parabolic surface viewed directly on from the direction of the Sun and all positions on the magnetopause surface account for aberration effects. The location at which MESSENGER passed through the magnetopause boundary (indicated by the vertical dashed red line in Figure 1) is marked by the black crosses in Figure 3 and the paraboloid's standoff distance was calculated using Equation 3 and this position. The color scale on the magnetopause surface in Figure 3 indicates the magnetic shear angle between

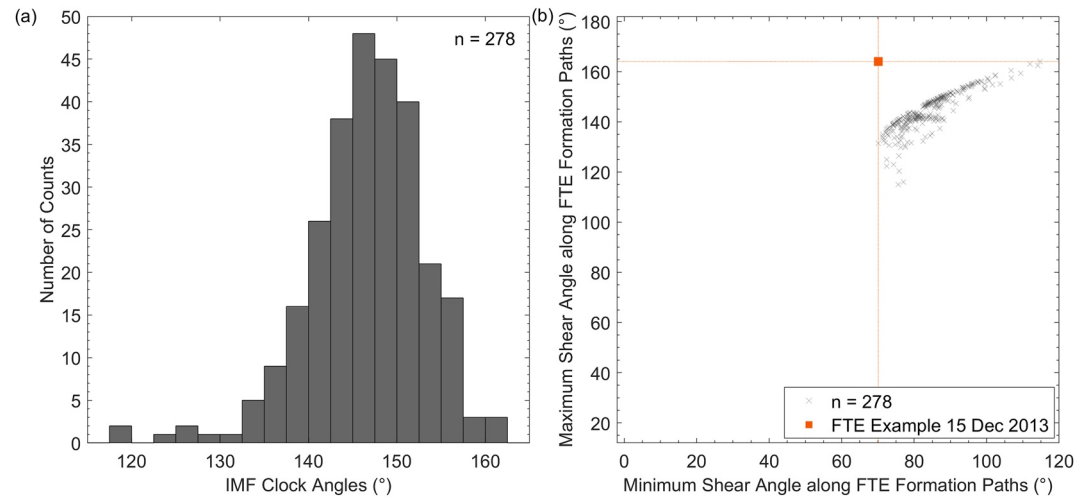


**Figure 4.** Statistics for the modeled FTE-type flux rope observed on 15 December 2013 shown in Figure 3. (a) Histogram of the IMF clock angles in the selected region upstream of the magnetopause (Figure 1b). (b) Scatter plot of the minimum and maximum shear angles along the traced FTE formation paths for each IMF clock angle orientation in panel (a). The orange square marks the absolute minimum and maximum shear angles along all formation paths for all IMF orientations, and the axis limits are selected to aid with later comparisons.

the draped magnetosheath field and the magnetospheric field either side of the boundary. The location at which MESSENGER observed the FTE-type FR is marked by the black dot on the magnetopause surface and the cyan lines show the FTE formation paths.

As can be seen in Figure 3, there are two modeled formation paths per IMF orientation for the FTE observed on 15 December 2013. These correspond to paths for the maximum and minimum values of the upstream solar wind conditions for the opened flux tube that is connected to only one cusp (determined from the FTE polarity)—we emphasize that they do not correspond to the initially considered paths (see Section 3) for the pair of opened flux tubes, each connected to the northern or southern cusp, as the polarity of the  $B_N$  signature has been taken into account. Since these paths were modeled by considering any uncertainties in the upstream solar wind conditions and the  $B_N$  signature's polarity, we assume the reconnection site that generated the FTE would have been located anywhere between these paths. In all three panels, the FTE formations paths can be seen to intersect with points of high-shear angle on the magnetopause surface. This is consistent with reconnection sites favoring higher shear regions on Earth's magnetopause (e.g., Phan et al., 2013). Additionally, the paths end at a point on the magnetopause, typically around the dayside subsolar point. This is due to points on the magnetopause surface where the two terms on the right-hand side of Equations 1 and 2 will be balanced. Hence, at these points, the FTE will have a net velocity of zero, and so, cannot move through or from this point on the magnetopause.

### 3.8. Statistics for the 15 December 2013 Event

Figure 4a shows a histogram of the IMF clock angles in the interval upstream of the magnetopause (Figure 1b). This histogram peaks around 145° to 150°, suggesting the observed FTE was most likely formed under near southward IMF conditions. Each of these IMF orientations were then input into our FR path model to generate a list of all the potential FTE formation paths, accounting for uncertainties in the upstream solar wind conditions. Using this list, we then determined values of the minimum and maximum shear angles between the reconnecting fields along both formation paths on the magnetopause surface for each of the IMF orientations.

A scatter plot of these minimum and maximum shear angles along all potential formation paths for each IMF orientation, are shown in Figure 4b. The absolute minimum and maximum shear angles along all formation paths for all IMF orientations is marked by the orange square, and the axis limits are selected to aid with later comparisons. As can be seen, the minimum clock angles cluster around 80°, suggesting that, given the upstream solar wind conditions were not known at the time of the FTE's observation, the FTE could potentially have formed under these lower shear conditions. However, the maximum shear angles along the FTE formation paths

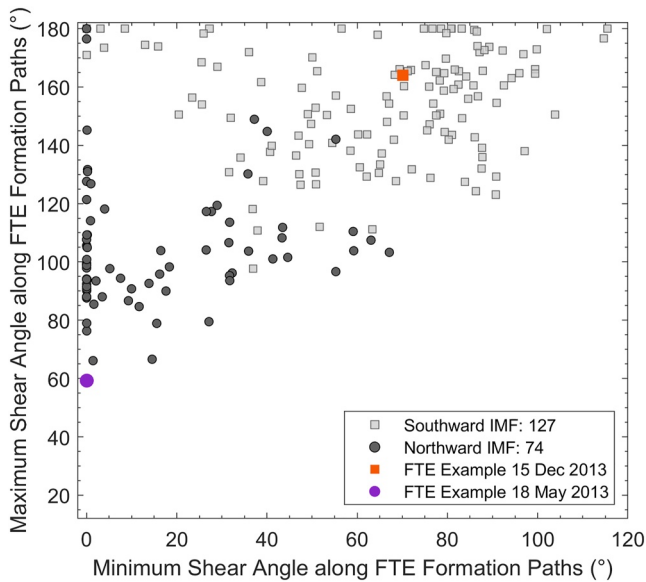


**Figure 5.** Scatter plot of the minimum against the maximum shear angles along the FTE formation paths for 201 MESSENGER inbound passes with steady IMF conditions binned by mean IMF orientation. Southward IMF (clock angles between  $90^\circ$  and  $270^\circ$ ) is marked by the light gray squares and Northward IMF (clock angles from  $0^\circ$  to  $90^\circ$  and  $270^\circ$  to  $360^\circ$ ) is marked by the dark gray circles. The larger purple circle and orange square highlight the maximum and minimum shear angles along the formation path for two example FTEs observed on 18 May 2013 and 15 December 2013 (shown in Figures 1, 3 and 4 and 6–8, respectively).

peak around  $140^\circ$ – $145^\circ$ . As the mean IMF clock angle in the relatively stable region upstream of the magnetopause was  $\sim 147^\circ$ , the magnetic shear angle pattern along the magnetopause in Figure 3b would suggest that the FTE's reconnection site was likely located in a region of higher magnetic shears on the dayside magnetopause. However, from Figure 4b it can be seen that the magnetic shear at the reconnection site was most likely to have been in the range of  $\sim 80^\circ$ – $145^\circ$ . This is consistent with studies at Earth that suggest reconnection sites favor points of higher shear on the magnetopause surface (e.g., Fuselier et al., 2021; Trattner et al., 2007).

#### 4. Statistical Results on Locations of Reconnection Sites

In Section 3, we outlined the method used to determine magnetic shear angles along the FTE formation paths for the FTE-type FR observed on 15 December 2013. These shear angles give information about the conditions under which reconnection-driven formation of the FTE took place. For the 15 December 2013 FTE-type FR, we found that the FTE was most likely to have formed in a region of higher magnetic shear on the magnetopause, which is consistent with studies at Earth (e.g., Phan et al., 2013). We then wanted to investigate if our 201 FTE-type FRs observed by MESSENGER during steady inbound passes were also consistent with this idea.

By applying the same method discussed in Section 3, for each of the 201 FTE-type FRs selected, we modeled formation paths under the minimum and maximum IMF clock angle orientations from the interval upstream of the magnetopause. Figures showing the modeled paths of these FTEs, similar to Figure 3, are included in Supporting Information S1, as well as an additional FTE observed on 11 April 2011 for comparison that was previously modeled in Slavin et al. (2012) but is not included in the statistics in this study as it did not meet our “steady” standard deviation threshold. Taking into account uncertainties in the upstream solar wind values and the polarities of the  $B_N$  signature, between 2 and 8 formation paths were deemed feasible for each of the FTEs with these IMF orientations. The minimum and maximum magnetic shear angles along the FTE formation paths were then found, giving an estimate for the most extreme values of the shear angle under which the reconnection-driven formation of the FTE-type FRs could have taken place.

Figure 5 shows a scatter plot of these minimum and maximum shear angles for all 201 FTEs. The scatter points are binned into two groups, “Southward” IMF orientations with clock angles between  $90^\circ$  to  $270^\circ$  and “Northward” IMF orientations with clock angles from  $0^\circ$  to  $90^\circ$  and  $270^\circ$  to  $360^\circ$ . As expected, FTEs in the Southward IMF group typically have high maximum shear angles along their paths, where “high” is deemed to be angles greater than  $135^\circ$ , and the maximum shear angles for the FTEs in the Northward IMF group are generally lower but the majority is above  $90^\circ$ . This is consistent with FTE formation reconnection sites favoring higher shear regions on the magnetopause. The minimum and maximum shear along the formation paths of the FTE observed on 15 December 2013 is marked by the orange square in Figure 5, as in Figure 4b. As can be seen in the figure, this FTE can be considered to be a fairly typical case, with relatively high minimum and maximum shear angles, reflective of the majority of the Southward IMF FTEs.

For the minimum shear angles along the Southward IMF FTE formation paths, the majority have angles greater than  $70^\circ$ . However, for both Northward and Southward IMF formation paths, minimum shear angles can get to as low as  $\sim 0^\circ$ . Whilst it is highly unlikely the reconnection that formed the observed FTEs occurred in a region of  $\sim 0^\circ$ , it is possible that reconnection-driven FTE formation could be taking place at locations on the magnetopause with lower shear angles than would be expected and the points of maximum shear on the magnetopause may not necessarily be favored.

In Figure 5, there are seven instances where, for Northward IMF formation paths, the maximum shear angle is less than  $80^\circ$  and three of these have maximum shear angles less than  $70^\circ$ . At Earth, Fear et al. (2007) highlighted one event where they found the maximum shear along an FTE path to be  $83^\circ$  and concluded the FTE was

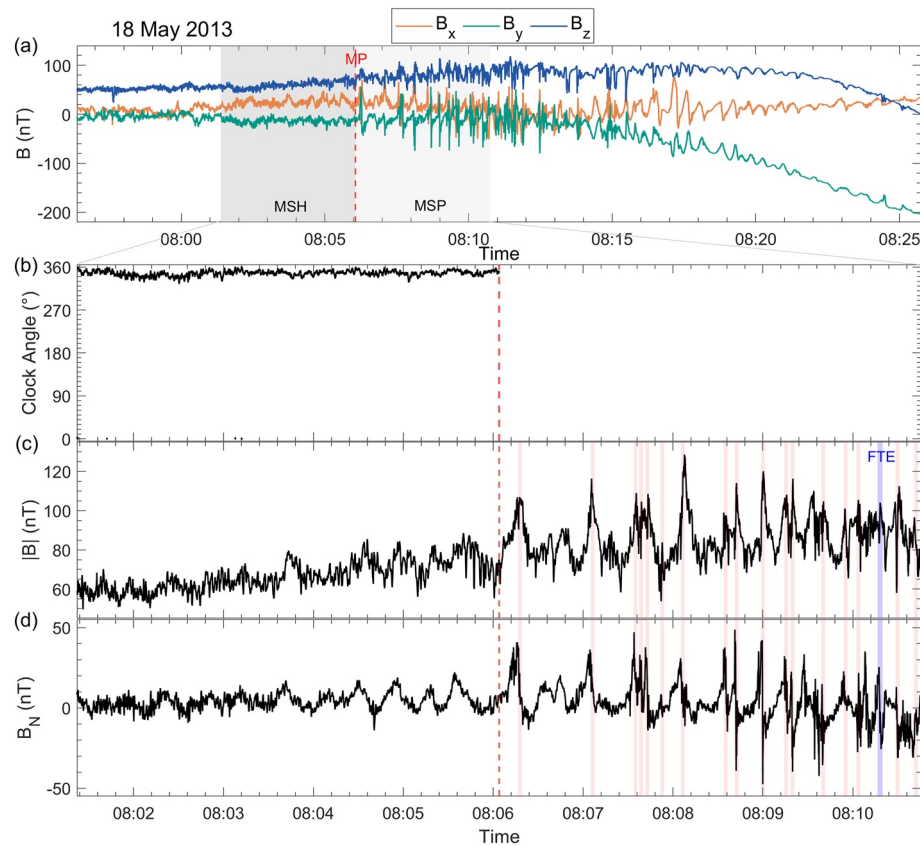


**Figure 6.** Additional example of a dayside inbound pass made by MESSANGER on 18 May 2013. Same as Figure 1.

formed at a component reconnection site. Therefore, the seven FTEs observed to have formed under low-shear reconnection conditions in this study were found to have magnetic shear angles lower than those at which reconnection has been typically observed to occur at Earth (e.g., Phan et al., 2013). Additionally, the majority of FTEs under Northward IMF have minimum shears along their paths at angles less than  $70^\circ$ , supporting previous work that shows low-shear reconnection, and hence FTE formation, could be occurring at Mercury's magnetopause (Dibraccio et al., 2013; Leyser et al., 2017; Slavin et al., 2014; Sun et al., 2020). In particular, for the FTE-type FR observed on 18 May 2013, highlighted by the purple circle in Figure 5, the absolute maximum shear angle along all feasible FTE formation paths is  $59^\circ$ . This suggests that this observed FTE could be providing good evidence of very low-magnetic shear reconnection occurring on Mercury's magnetopause. Therefore, a more detailed discussion of this event is provided in the following section.

### 5. Evidence of Low-Shear Reconnection on Mercury's Magnetopause: 18 May 2013 FTE Case Study

As discussed in the previous section, the FTE-type FR observed on 18 May 2013 appeared to show good evidence that this FTE was formed under low-shear reconnection conditions on Mercury's magnetopause. Just as in Figure 1, Figure 6 shows time series of magnetic field measurements made during MESSANGER's inbound pass on 18 May 2013, where the magnetopause crossing is marked by the vertical dashed red line and was determined using the observed change in the average magnetic field strength, based on a 30-s window centered around each point. Figures 6c and 6d show the magnetic field magnitude ( $|B|$ ) as measured by MESSANGER and the magnetic field component projected in the direction normal to the magnetopause surface ( $B_N$ ). The vertical red and blue lines in Figures 6c and 6d mark the FTE-type FRs, identified by a bipolar signature in  $B_N$  and an enhancement in  $|B|$ , and the polarities of these FTEs are standard (+ to -).

We apply the same modeling framework as that discussed in Section 3 and Figure 7 shows the modeled locations of the reconnection sites for the FTE observed on 18 May 2013. Figures 7a–7c, show the modeled FTE



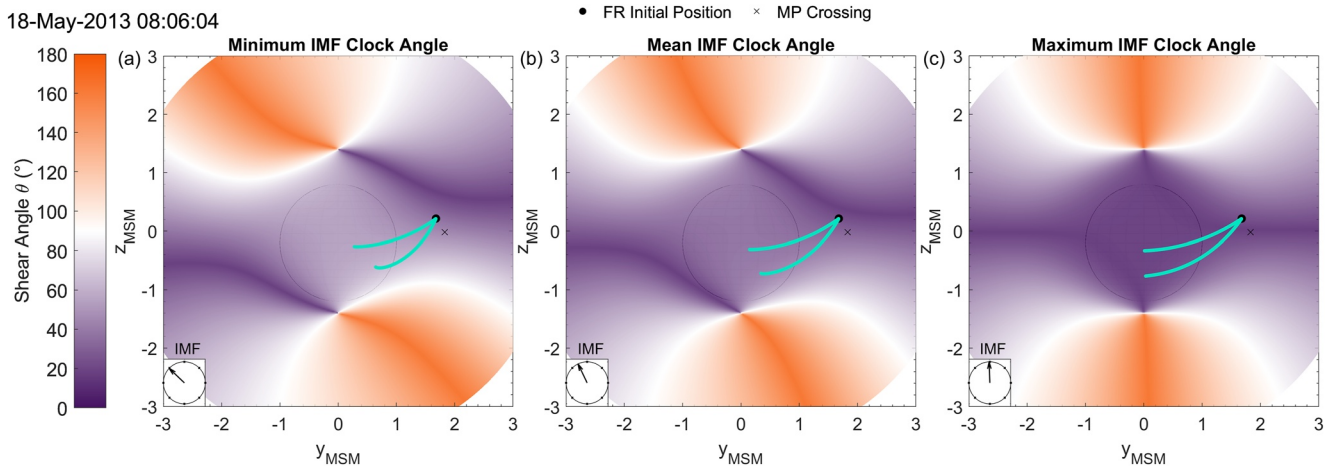


**Figure 7.** FTE-type flux rope formation paths modeled backwards in time on Mercury's magnetopause surface viewed from along the upstream solar wind flow direction using parameters measured by MESSENGER on 18 May 2013. Same as Figure 3.

formation paths for the minimum, mean and maximum clock angle orientations of the IMF in the region upstream of the magnetopause (Figure 6b). For each IMF orientation, there are two paths that the FTE could have formed anywhere in between, deemed feasible from the  $B_N$  signature polarity and taking into account uncertainties in the upstream solar wind values. It is evident from Figure 7 that the FTE formation paths do not intersect with regions of maximal shear on the magnetopause as would be expected. Instead, the paths appear to pass through regions of very low shear around the subsolar point, with a maximum shear angle along all of these paths of only  $59^\circ$ .

At Earth, local lower shear magnetic reconnection has been observed (e.g., Chandler et al., 1999; Escoubet et al., 2008; Fuselier et al., 1997; Gosling et al., 1990; Onsager & Fuselier, 1994; Sandholt et al., 1998; Trattner et al., 2017; Wing et al., 2001; Øieroset et al., 1997). However, to get an idea of global magnetic reconnection, a dominant X-line is typically traced by following points of maximum shear across the magnetopause surface (Dungey, 1961; Fuselier et al., 2021; Sonnerup et al., 1981). Often this leads to a tilted X-line that connects two regions of high-shear in the northern and southern hemispheres across the subsolar region (Trattner et al., 2007). Employing a similar approach for the modeled FTE shown in Figure 7, the regions of higher shear in the northern dawn and southern dusk sectors would result in a tilted X-line that passes through an area of very low-shear around the subsolar region that may be more difficult to justify. This may suggest that, at Mercury, global magnetic reconnection is less restricted to points of maximal shear on the magnetopause, instead occurring at points across the dayside magnetopause surface, and could call into question whether the Trattner et al. (2007) dominant X-line model, frequently used at Earth, is as applicable in the very different system of Mercury.

In Figure 8a, a histogram of the IMF clock angles in the interval upstream of the magnetopause (Figure 6b) for the 18 May 2013 event, similar to Figure 4a, is shown. As the histogram peaks around  $345^\circ$  to  $350^\circ$  and the range of IMF values is from  $330^\circ$  to  $360^\circ$ , the observed FTE likely formed under near northward IMF, and hence low-magnetic shear, conditions. For each IMF orientation in the histogram in Figure 8a, we modeled the potential FR formation paths, whilst accounting for upstream solar wind uncertainties. For each IMF orientation, values of the minimum and maximum shear angles between the reconnecting fields along all of the potential formation paths on the magnetopause surface were determined. Figure 8b shows a scatter plot of these minimum and maximum shear angles, with the most extreme values marked by the purple circle, as in Figure 5. For the FTE-type FR observed on 18 May 2013, the absolute maximum value of the shear angle along any of the formation paths was  $59^\circ$ . However, the minimum shear angles along the FTE paths for each IMF orientation can be seen to peak around  $5^\circ$  and the maximum peaks around  $35^\circ$ . This would suggest that whilst the FTE could have formed under reconnection conditions at a shear angle of  $\sim 59^\circ$ , it is much more likely that this FTE-type was formed at a reconnection site with an even lower magnetic shear angle.

Additionally, MESSENGER observed 17 other FTE-type FRs during the same inbound pass of the magnetosphere on 18 May 2013, see red vertical lines in Figures 6c and 6d. Therefore, it can be argued that it is unlikely the FTE modeled in Figures 7 and 8 were coincidentally formed under local conditions that differed significantly from the globally modeled picture. Instead, this FTE-type FR supports the hypothesis that magnetic reconnection



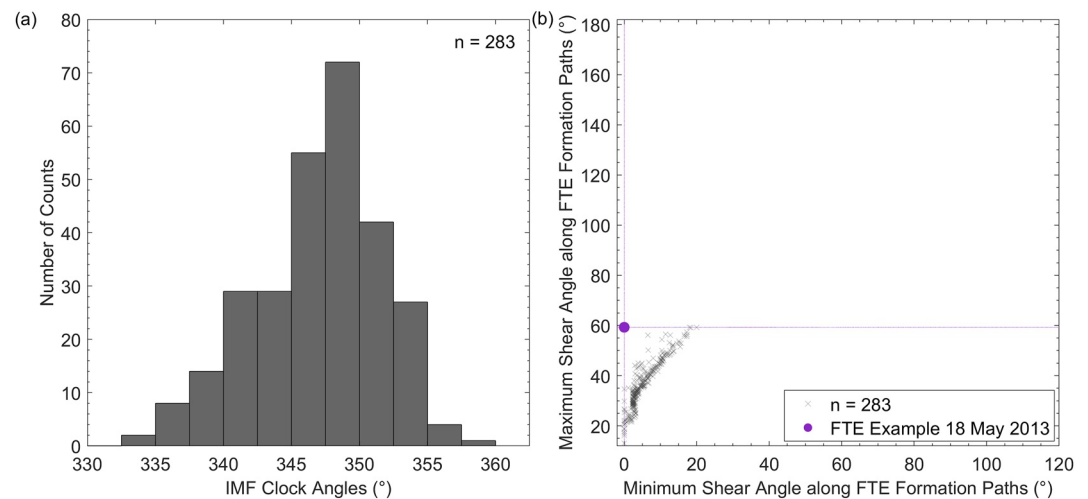


**Figure 8.** Statistics for the modeled FTE-type flux rope observed on 18 May 2018 shown in Figure 7. Same as Figure 4.

can occur on Mercury's magnetopause much more easily than at Earth (e.g., Dibraccio et al., 2013) and under very low-magnetic shear conditions.

## 6. Conclusions

In this study, we analyzed 201 FTEs formed under relatively stable upstream solar wind conditions as observed by MESSENGER during inbound magnetopause crossings. Using the approach of Cooling et al. (2001), but tracking the FTE-type FRs backwards in time, we modeled FTE formation paths on the magnetopause between which are reconnection sites where the observed FTE-type FRs were likely generated. It was found that for the majority of the 201 FTEs, the maximum shear angle along their formation paths was greater than  $135^\circ$ . However, seven FTE-type FRs were found where the maximum shear angle possible along their paths was less than  $80^\circ$  and three of these had maximum shear angles less than  $70^\circ$ . Investigating this further, we found the FTE observed on 18 May 2013 had a maximum shear angle of  $59^\circ$  and, more likely, was formed at a reconnection site with an even lower magnetic shear angle. These FTE examples provide good evidence of very low-shear magnetic reconnection occurring on Mercury's magnetopause. This supports the hypothesis that symmetric reconnection dominates at Mercury's dayside magnetopause and diamagnetic drift will interfere less with reconnection processes, leading to enhanced reconnection driven FTE formation that can occur over a larger range of shear angles than those typically observed at Earth. Additionally, for the FTEs formed under these low-shear reconnection conditions, tracing a dominant X-line that connects points of maximum shear along the magnetopause may be more difficult to justify as it would pass through a region of very low-shear on the magnetopause. This leads us to the questions, is reconnection confined to the dominant X-line only on Mercury's magnetopause? Or can reconnection occur much more easily across Mercury's magnetopause and at points that do not maximize the magnetic shear angle? With the arrival of the BepiColombo mission in 2025 (Benkhoff et al., 2021; Heyner et al., 2021; Milillo et al., 2020), and particularly with the dual spacecraft nature of the mission, additional observations of FTEs occurring under Northward IMF conditions and, hence, low-magnetic shear may help to answer these remaining questions.

## Data Availability Statement

Calibrated magnetic field data from the MESSENGER mission are available from the Planetary Plasma Interaction (PPI) Node of NASA's Planetary Data System (PDS) (<https://pds-ppi.igpp.ucla.edu/>) in the folder MESS-E/V/H/SW-MAG-3-CDR-CALIBRATED-V1.0. Derived data shown in Figures 3–5 and 7–8 are publicly available in the Zenodo data repository (<https://doi.org/10.5281/zenodo.8325368>) with Creative Commons Attribution (Zomerdiik-Russell, Masters, Sun, et al., 2023).

**Acknowledgments**

S.Z.-R. is supported by an STFC Studentship 2439770. A.M. is supported by a Royal Society University Research Fellowship. R.C.F. is supported by an STFC Consolidated Grant ST/V000942/1. W.S. and J.A.S. are supported by NASA Grant 80NSSC21K0052 and Discovery Data Analysis Program Grant 80NSSC22K1061.

**References**

Alexeev, I. I., Belenkaya, E. S., Bobrovnikov, S. Y., Slavin, J. A., & Sarantos, M. (2008). Paraboloid model of Mercury's magnetosphere. *Journal of Geophysical Research*, *113*(12), A12210. <https://doi.org/10.1029/2008JA013368>

Anderson, B. J., Acuña, M. H., Korth, H., Purucker, M. E., Johnson, C. L., Slavin, J. A., et al. (2008). The structure of Mercury's magnetic field from MESSENGER's first flyby. *Science*, *321*(5885), 82–85. <https://doi.org/10.1126/science.1159081>

Anderson, B. J., Johnson, C. L., Korth, H., Winslow, R. M., Borovsky, J. E., Purucker, M. E., et al. (2012). Low-degree structure in Mercury's planetary magnetic field. *Journal of Geophysical Research E: Planets*, *117*(12), E00L12. <https://doi.org/10.1029/2012JE004159>

Benkhoff, J., Murakami, G., Baumjohann, W., Besse, S., Bunce, E., Casale, M., et al. (2021). BepiColombo—Mission overview and science goals. *Space Science Reviews*, *217*(8), 90. <https://doi.org/10.1007/s11214-021-00861-4>

Chandler, M. O., Fuselier, S. A., Lockwood, M., & Moore, T. E. (1999). Evidence of component merging equatorward of the cusp. *Journal of Geophysical Research*, *104*(A10), 22623–22633. <https://doi.org/10.1029/1999JA900175>

Cooling, B. M. A., Owen, C. J., & Schwartz, S. J. (2001). Role of the magnetosheath flow in determining the motion of open flux tubes. *Journal of Geophysical Research*, *106*(A9), 18763–18775. <https://doi.org/10.1029/2000ja000455>

Cowley, S. W. H., & Owen, C. J. (1989). A simple illustrative model of open flux tube motion over the dayside magnetopause. *Planetary and Space Science*, *37*(11), 1461–1475. [https://doi.org/10.1016/0032-0633\(89\)90116-5](https://doi.org/10.1016/0032-0633(89)90116-5)

de Hoffmann, F., & Teller, E. (1950). Magneto-hydrodynamic shocks. *Physical Review*, *80*(4), 692–703. <https://doi.org/10.1103/PhysRev.80.692>

Dibraccio, G. A., Slavin, J. A., Boardsen, S. A., Anderson, B. J., Korth, H., Zurbuchen, T. H., et al. (2013). MESSENGER observations of magnetopause structure and dynamics at Mercury. *Journal of Geophysical Research: Space Physics*, *118*(3), 997–1008. <https://doi.org/10.1002/jgra.50123>

Diego, P., Piersanti, M., Laurenza, M., & Villante, U. (2020). Properties of solar wind structures at Mercury's orbit. *Journal of Geophysical Research: Space Physics*, *125*(9), e2020JA028281. <https://doi.org/10.1029/2020JA028281>

Dungey, J. W. (1961). Interplanetary magnetic field and the auroral zones. *Physical Review Letters*, *6*(2), 47–48. <https://doi.org/10.1103/PhysRevLett.6.47>

Escoubet, C. P., Berchem, J., Bosqued, J. M., Trattner, K. J., Taylor, M. G. G. T., Pitout, F., et al. (2008). Two sources of magnetosheath ions observed by Cluster in the mid-altitude polar cusp. *Advances in Space Research*, *41*(10), 1528–1536. <https://doi.org/10.1016/j.asr.2007.04.031>

Fear, R. C., Milan, S. E., Fazakerley, A. N., Fornaçon, K.-H., Carr, C. M., & Dandouras, I. (2009). Simultaneous observations of flux transfer events by THEMIS, cluster, double star, and SuperDARN: Acceleration of FTEs. *Journal of Geophysical Research*, *114*(A10), A10213. <https://doi.org/10.1029/2009JA014310>

Fear, R. C., Milan, S. E., Fazakerley, A. N., Owen, C. J., Asikainen, T., Taylor, M. G. G. T., et al. (2007). Motion of flux transfer events: A test of the cooling model. *Annales Geophysicae*, *25*(7), 1669–1690. <https://doi.org/10.5194/angeo-25-1669-2007>

Fuselier, S. A., Anderson, B. J., & Onsager, T. G. (1997). Electron and ion signatures of field line topology at the low-shear magnetopause. *Journal of Geophysical Research*, *102*(A3), 4847–4863. <https://doi.org/10.1029/96JA03635>

Fuselier, S. A., Webster, J. M., Trattner, K. J., Petrinc, S. M., Genestreti, K. J., Pritchard, K. R., et al. (2021). Reconnection X-line orientations at the Earth's magnetopause. *Journal of Geophysical Research: Space Physics*, *126*(12), e2021JA029789. <https://doi.org/10.1029/2021JA029789>

Gershman, D. J., Slavin, J. A., Raines, J. M., Zurbuchen, T. H., Anderson, B. J., Korth, H., et al. (2013). Magnetic flux pileup and plasma depletion in Mercury's subsolar magnetosheath. *Journal of Geophysical Research: Space Physics*, *118*(11), 7181–7199. <https://doi.org/10.1002/2013JA019244>

Gosling, J. T., Thomsen, M. F., Bame, S. J., Elphic, R. C., & Russell, C. T. (1990). Cold ion beams in the low latitude boundary layer during accelerated flow events. *Geophysical Research Letters*, *17*(12), 2245–2248. <https://doi.org/10.1029/GL0171012p02245>

Guo, J., Lu, S., Lu, Q., Lin, Y., Wang, X., Huang, K., et al. (2021). Re-reconnection processes of magnetopause flux ropes: Three-dimensional global hybrid simulations. *Journal of Geophysical Research: Space Physics*, *126*(6), e2021JA029388. <https://doi.org/10.1029/2021JA029388>

Haerendel, G., Paschmann, G., Scokopke, N., Rosenbauer, H., & Hedgecock, P. C. (1978). The frontside boundary layer of the magnetosphere and the problem of reconnection. *Journal of Geophysical Research*, *83*(A7), 3195–3216. <https://doi.org/10.1029/JA083iA07p03195>

Heyner, D., Auster, H.-U., Fornaçon, K.-H., Carr, C., Richter, I., Mieth, J. Z. D., et al. (2021). The BepiColombo planetary magnetometer MPO-MAG: What can we learn from the Hermean magnetic field? *Space Science Reviews*, *217*(4), 52. <https://doi.org/10.1007/s11214-021-00822-x>

Heyner, D., Nabert, C., Liebert, E., & Glassmeier, K. H. (2016). Concerning reconnection-induction balance at the magnetopause of Mercury. *Journal of Geophysical Research A: Space Physics*, *121*(4), 2935–2961. <https://doi.org/10.1002/2015JA021484>

Imber, S. M., Slavin, J. A., Boardsen, S. A., Anderson, B. J., Korth, H., McNutt, R. L., Jr., & Solomon, S. C. (2014). MESSENGER observations of large dayside flux transfer events: Do they drive Mercury's substorm cycle? *Journal of Geophysical Research: Space Physics*, *119*(7), 5613–5623. <https://doi.org/10.1002/2014JA019884>

Jasinski, J. M., Akhavan-Tafti, M., Sun, W., Slavin, J. A., Coates, A. J., Fuselier, S. A., et al. (2021). Flux transfer events at a reconnection-suppressed magnetopause: Cassini observations at Saturn. *Journal of Geophysical Research: Space Physics*, *126*(2), e2020JA028786. <https://doi.org/10.1029/2020JA028786>

Jasinski, J. M., Slavin, J. A., Arridge, C. S., Poh, G., Jia, X., Sergis, N., et al. (2016). Flux transfer event observation at Saturn's dayside magnetopause by the Cassini spacecraft. *Geophysical Research Letters*, *43*(13), 6713–6723. <https://doi.org/10.1002/2016GL069260>

Johnson, C. L., Purucker, M. E., Korth, H., Anderson, B. J., Winslow, R. M., Al Asad, M. M. H., et al. (2012). MESSENGER observations of Mercury's magnetic field structure. *Journal of Geophysical Research E: Planets*, *117*(12), E00L14. <https://doi.org/10.1029/2012JE004217>

Kobel, E., & Flückiger, E. O. (1994). A model of the steady state magnetic field in the magnetosheath. *Journal of Geophysical Research*, *99*(12), 23617–23622. <https://doi.org/10.1029/94JA01778>

Lee, L. C., & Fu, Z. F. (1985). A theory of magnetic flux transfer at the Earth's magnetopause. *Geophysical Research Letters*, *12*(2), 105–108. <https://doi.org/10.1029/GL012i002p00105>

Leyser, R. P., Imber, S. M., Milan, S. E., & Slavin, J. A. (2017). The influence of IMF clock angle on dayside flux transfer events at Mercury. *Geophysical Research Letters*, *44*(21), 10829–10837. <https://doi.org/10.1002/2017GL074858>

Li, C., Jia, X., Chen, Y., Toth, G., Zhou, H., Slavin, J. A., et al. (2023). Global hall MHD simulations of Mercury's magnetopause dynamics and FTEs under different solar wind and IMF conditions. *Journal of Geophysical Research: Space Physics*, *128*(5), e2022JA031206. <https://doi.org/10.1029/2022JA031206>

Lockwood, M., Cowley, S. W. H., Smith, M. F., Rijnbeek, R. P., & Elphic, R. C. (1995). The contribution of flux transfer events to convection. *Geophysical Research Letters*, *22*(10), 1185–1188. <https://doi.org/10.1029/95GL01008>

Lu, Q., Guo, J., Lu, S., Wang, X., Slavin, J. A., Sun, W., et al. (2022). Three-dimensional global hybrid simulations of flux transfer event showers at Mercury. *The Astrophysical Journal*, *937*(1), 1. <https://doi.org/10.3847/1538-4357/ac8bfc>

- Masters, A. (2014). Magnetic reconnection at Uranus' magnetopause. *Journal of Geophysical Research: Space Physics*, 119(7), 5520–5538. <https://doi.org/10.1002/2014JA020077>
- Milillo, A., Fujimoto, M., Murakami, G., Benkhoff, J., Zender, J., Aizawa, S., et al. (2020). Investigating Mercury's environment with the two-spacecraft BepiColombo mission. *Space Science Reviews*, 216(5), 93. <https://doi.org/10.1007/s11214-020-00712-8>
- Ness, N. F., Behannon, K. W., Lepping, R. P., & Whang, Y. C. (1975). The magnetic field of Mercury, 1. *Journal of Geophysical Research*, 80(19), 2708–2716. <https://doi.org/10.1029/ja080i019p02708>
- Ness, N. F., Behannon, K. W., Lepping, R. P., Whang, Y. C., & Schatten, K. H. (1974). Magnetic field observations near Mercury: Preliminary results from mariner 10. *Science*, 183(4146), 151–160. <https://doi.org/10.1126/science.185.4146.151>
- Øieroset, M., Sandholt, P. E., Denig, W. F., & Cowley, S. W. H. (1997). Northward interplanetary magnetic field cusp aurora and high-latitude magnetopause reconnection. *Journal of Geophysical Research*, 102(A6), 11349–11362. <https://doi.org/10.1029/97JA00559>
- Onsager, T. G., & Fuselier, S. A. (1994). The location of magnetopause reconnection for northward and southward interplanetary magnetic field. *Washington DC American Geophysical Union Geophysical Monograph Series*, 84, 183–197. <https://doi.org/10.1029/GM084p0183>
- Paschmann, G., Papamastorakis, I., Baumjohann, W., Sckopke, N., Carlson, C. W., Sonnerup, B. U. Ö., & Lühr, H. (1986). The magnetopause for large magnetic shear: AMPTE/IRM observations. *Journal of Geophysical Research*, 91(A10), 11099–11115. <https://doi.org/10.1029/JA091iA10p11099>
- Petrinec, S. M., & Russell, C. T. (1997). Hydrodynamic and MHD equations across the bow shock and along the surfaces of planetary obstacles. *Space Science Reviews*, 79(3/4), 757–791. <https://doi.org/10.1023/a:1004938724300>
- Phan, T. D., Gosling, J. T., Paschmann, G., Pasma, C., Drake, J. F., Øieroset, M., et al. (2010). The dependence of magnetic reconnection on plasma  $\beta$  and magnetic shear: Evidence from solar wind observations. *The Astrophysical Journal*, 719(2), L199–L203. <https://doi.org/10.1088/2041-8205/719/2/L199>
- Phan, T. D., Paschmann, G., Gosling, J. T., Øieroset, M., Fujimoto, M., Drake, J. F., & Angelopoulos, V. (2013). The dependence of magnetic reconnection on plasma  $\beta$  and magnetic shear: Evidence from magnetopause observations. *Geophysical Research Letters*, 40(1), 11–16. <https://doi.org/10.1029/2012GL054528>
- Raeder, J. (2006). Flux transfer events: 1. Generation mechanism for strong southward IMF. *Annales Geophysicae*, 24(1), 381–392. <https://doi.org/10.5194/angeo-24-381-2006>
- Rijnbeek, R. P., Cowley, S. W. H., Southwood, D. J., & Russell, C. T. (1982). Observations of reverse polarity flux transfer events at the Earth's dayside magnetopause. *Nature*, 300(5887), 5887–5926. <https://doi.org/10.1038/300023a0>
- Russell, C. T., & Elphic, R. C. (1978). Initial ISEE magnetometer results: Magnetopause observations. *Space Science Reviews*, 22(6), 681–715. <https://doi.org/10.1007/BF00212619>
- Russell, C. T., & Walker, R. J. (1985). Flux transfer events at Mercury. *Journal of Geophysical Research*, 90(A11), 11067–11074. <https://doi.org/10.1029/ja090ia11p11067>
- Sandholt, P. E., Farrugia, C. J., Moen, J., Norberg, Ø., Lybekk, B., Sten, T., & Hansen, T. (1998). A classification of dayside auroral forms and activities as a function of interplanetary magnetic field orientation. *Journal of Geophysical Research*, 103(A10), 23325–23345. <https://doi.org/10.1029/98JA02156>
- Slavin, J. A., Lepping, R. P., Wu, C. C., Anderson, B. J., Baker, D. N., Benna, M., et al. (2010b). MESSENGER observations of large flux transfer events at mercury. *Geophysical Research Letters*, 37(2), L02105. <https://doi.org/10.1029/2009GL041485>
- Slavin, J. A., Acuña, M. H., Anderson, B. J., Baker, D. N., Benna, M., Boardsen, S. A., et al. (2009). MESSENGER observations of magnetic reconnection in Mercury's Magnetosphere. *Science*, 324(5927), 606–610. <https://doi.org/10.1126/science.1172011>
- Slavin, J. A., Anderson, B. J., Baker, D. N., Benna, M., Boardsen, S. A., Gloeckler, G., et al. (2010a). MESSENGER observations of extreme loading and unloading of mercury's magnetic tail. *Science*, 329(5992), 665–668. <https://doi.org/10.1126/science.1188067>
- Slavin, J. A., Dibaccio, G. A., Gershman, D. J., Imber, S. M., Poh, G. K., Raines, J. M., et al. (2014). MESSENGER observations of Mercury's dayside magnetosphere under extreme solar wind conditions. *Journal of Geophysical Research: Space Physics*, 119(10), 8087–8116. <https://doi.org/10.1002/2014JA020319>
- Slavin, J. A., & Holzer, R. E. (1979). The effect of erosion on the solar wind stand-off distance at Mercury. *Journal of Geophysical Research*, 84(A5), 2076–2082. <https://doi.org/10.1029/JA084iA05p02076>
- Slavin, J. A., Imber, S. M., Boardsen, S. A., Di Braccio, G. A., Sundberg, T., Sarantos, M., et al. (2012). MESSENGER observations of a flux-transfer-event shower at Mercury. *Journal of Geophysical Research*, 117(10), A00M06. <https://doi.org/10.1029/2012JA017926>
- Slavin, J. A., Imber, S. M., & Raines, J. M. (2021). A dungey cycle in the life of mercury's magnetosphere. In *Magnetospheres in the solar system* (pp. 535–556). American Geophysical Union (AGU). <https://doi.org/10.1002/9781119815624.ch34>
- Smith, A. W., Jackman, C. M., Frohmaier, C. M., Coxon, J. C., Slavin, J. A., & Fear, R. C. (2018). Evaluating single-spacecraft observations of planetary magnetotails with simple Monte Carlo simulations: 1. Spatial distributions of the neutral line. *Journal of Geophysical Research: Space Physics*, 123(12), 10109–10123. <https://doi.org/10.1029/2018JA025958>
- Smith, A. W., Jackman, C. M., Frohmaier, C. M., Fear, R. C., Slavin, J. A., & Coxon, J. C. (2018). Evaluating single spacecraft observations of planetary magnetotails with simple Monte Carlo simulations: 2. Magnetic flux rope signature selection effects. *Journal of Geophysical Research: Space Physics*, 123(12), 10124–10138. <https://doi.org/10.1029/2018JA025959>
- Smith, A. W., Slavin, J. A., Jackman, C. M., Fear, R. C., Poh, G.-K., DiBraccio, G. A., et al. (2017). Automated force-free flux rope identification. *Journal of Geophysical Research: Space Physics*, 122(1), 780–791. <https://doi.org/10.1002/2016JA022994>
- Smith, A. W., Slavin, J. A., Jackman, C. M., Poh, G.-K., & Fear, R. C. (2017). Flux ropes in the Hermean magnetotail: Distribution, properties, and formation. *Journal of Geophysical Research: Space Physics*, 122(8), 8136–8153. <https://doi.org/10.1002/2017JA024295>
- Solomon, S. C., McNutt, R. L., Gold, R. E., & Domingue, D. L. (2007). MESSENGER mission overview. *Space Science Reviews*, 131(1–4), 3–39. <https://doi.org/10.1007/s11214-007-9247-6>
- Sonnerup, B. U. Ö., Paschmann, G., Papamastorakis, I., Sckopke, N., Haerendel, G., Bame, S. J., et al. (1981). Evidence for magnetic field reconnection at the Earth's magnetopause. *Journal of Geophysical Research*, 86(A12), 10049–10067. <https://doi.org/10.1029/JA086iA12p10049>
- Sonnerup, B. U. Ö. (1974). Magnetopause reconnection rate. *Journal of Geophysical Research*, 79(10), 1546–1549. <https://doi.org/10.1029/JA079i010p01546>
- Sun, W.-J., Dewey, R. M., Aizawa, S., Huang, J., Slavin, J. A., Fu, S., et al. (2022). Review of Mercury's dynamic magnetosphere: Post-MESSENGER era and comparative magnetospheres. *Science China Earth Sciences*, 65(1), 25–74. <https://doi.org/10.1007/s11430-021-9828-0>
- Sun, W.-J., Slavin, J. A., Smith, A. W., Dewey, R. M., Poh, G. K., Jia, X., et al. (2020). Flux transfer event showers at Mercury: Dependence on plasma  $\beta$  and magnetic shear and their contribution to the dungey cycle. *Geophysical Research Letters*, 47(21), e2020GL089784. <https://doi.org/10.1029/2020GL089784>
- Swisdak, M., & Drake, J. F. (2007). Orientation of the reconnection X-line. *Geophysical Research Letters*, 34(11), L11106. <https://doi.org/10.1029/2007GL029815>

- Swisdak, M., Opher, M., Drake, J. F., & Alouani Bibi, F. (2010). The vector direction of the interstellar magnetic field outside the heliosphere. *The Astrophysical Journal*, *710*(2), 1769–1775. <https://doi.org/10.1088/0004-637X/710/2/1769>
- Swisdak, M., Rogers, B. N., Drake, J. F., & Shay, M. A. (2003). Diamagnetic suppression of component magnetic reconnection at the magnetopause. *Journal of Geophysical Research*, *108*(A5), 1218. <https://doi.org/10.1029/2002JA009726>
- Trattner, K. J., Mulcock, J. S., Petrinec, S. M., & Fuselier, S. A. (2007). Probing the boundary between antiparallel and component reconnection during southward interplanetary magnetic field conditions. *Journal of Geophysical Research*, *112*(A8), A08210. <https://doi.org/10.1029/2007JA012270>
- Trattner, K. J., Thresher, S., Trenchi, L., Fuselier, S. A., Petrinec, S. M., Peterson, W. K., & Marcucci, M. F. (2017). On the occurrence of magnetic reconnection equatorward of the cusps at the Earth's magnetopause during northward IMF conditions. *Journal of Geophysical Research: Space Physics*, *122*(1), 605–617. <https://doi.org/10.1002/2016JA023398>
- Vandas, M., Němeček, Z., Šafránková, J., Romashets, E. P., & Hajoš, M. (2020). Comparison of observed and modeled magnetic fields in the Earth's magnetosheath. *Journal of Geophysical Research: Space Physics*, *125*(3), e2019JA027705. <https://doi.org/10.1029/2019JA027705>
- Walker, R. J., & Russell, C. T. (1985). Flux transfer events at the Jovian magnetopause. *Journal of Geophysical Research*, *90*(A8), 7397–7404. <https://doi.org/10.1029/JA090iA08p07397>
- Wing, S., Newell, P. T., & Ruohoniemi, J. M. (2001). Double cusp: Model prediction and observational verification. *Journal of Geophysical Research*, *106*(A11), 25571–25593. <https://doi.org/10.1029/2000JA000402>
- Winslow, R. M., Anderson, B. J., Johnson, C. L., Slavin, J. A., Korth, H., Purucker, M. E., et al. (2013). Mercury's magnetopause and bow shock from MESSENGER Magnetometer observations. *Journal of Geophysical Research: Space Physics*, *118*(5), 2213–2227. <https://doi.org/10.1002/jgra.50237>
- Zhong, J., Wan, W. X., Wei, Y., Slavin, J. A., Raines, J. M., Rong, Z. J., et al. (2015). Compressibility of Mercury's dayside magnetosphere. *Geophysical Research Letters*, *42*(23), 10135–10139. <https://doi.org/10.1002/2015GL067063>
- Zomerdijk-Russell, S., Masters, A., & Heyner, D. (2021). Variability of the interplanetary magnetic field as a driver of electromagnetic induction in Mercury's interior. *Journal of Geophysical Research: Space Physics*, *126*(10), e2021JA029664. <https://doi.org/10.1029/2021ja029664>
- Zomerdijk-Russell, S., Masters, A., Korth, H., & Heyner, D. (2023). Modeling the time-dependent magnetic fields that BepiColombo will use to probe down into Mercury's mantle. *Geophysical Research Letters*, *50*(2), e2022GL101607. <https://doi.org/10.1029/2022GL101607>
- Zomerdijk-Russell, S., Masters, A., Sun, W. J., Fear, R. C., & Slavin, J. A. (2023). Derived data for: “Does reconnection only occur at points of maximum shear on Mercury's dayside magnetopause?” [Dataset]. Zenodo. <https://doi.org/10.5281/zenodo.8325368>